Consolidation of Carbon Nanotube Reinforced Aluminum Matrix Composites by High-Pressure Torsion

HAMED ASGHARZADEH, SOO-HYUN JOO, and HYOUNG SEOP KIM

Al-3 vol pct carbon nanotube (CNT) composites are fabricated by consolidation through high-pressure torsion (HPT) at room temperature. The densification behavior, microstructural evolution, and mechanical properties of Al/CNT composites are studied. The results show that density and microstructural homogeneity increase with increasing number of revolutions under a high pressure of 6 GPa. Substantial grain refinement is achieved after 10 turns of HPT with an average grain thickness of ~38 nm perpendicular to the compression axis of HPT. The Al/CNT composite shows a considerable increase in hardness and strength compared to the Al matrix. The strengthening mechanisms of the Al/CNT composite are found to be (i) grain refinement of Al matrix and (ii) Orowan looping. Raman spectroscopy and high-resolution transmission electron microscopy reveal that the structure of most of CNTs is changed during processing through mechanical milling and HPT.

DOI: 10.1007/s11661-014-2354-6

I. INTRODUCTION

CARBON nanotubes (CNTs) have unique tubular structures with a few nanometer diameter and large aspect ratio that possess high elastic modulus (>1 TPa) and high tensile strength (>30 GPa).[1] These exceptional mechanical properties combined with a low density make them an ideal reinforcement in Al matrix composites (AMCs) for the automotive and aerospace industries where weight reduction for decreasing fuel consumption is a priority. However, CNTs have a strong tendency to agglomerate due to their high aspect ratio and their Van der Waals bondings.[2] This agglomeration is detrimental to the mechanical properties of AMCs and is a major challenge that inhibits the development of these composites. Many methods have been used in an effort to reduce the agglomeration of CNTs: coating CNTs on the Al powder surface,[3] *in situ* synthesis of CNTs in Al powders,[4] molecular level mixing of the CNT/Cu composite with Al powders,[5] and mechanical milling (MM) of Al/CNT powder mixtures.[6] MM, a solid state high-energy ball milling process that introduces a reinforcement phase into the matrix by repeated cycles of welding-fracture-welding of the particles,[7] has been used successfully to uniformly disperse a variety of reinforcements within an Al matrix.[8–10] Furthermore, the mechanical properties of a MM processed Al/CNT composite would be further improved by the Al grain refinement to the nanoscale due to intense straining and by the incorporation and dispersion of the oxide layer initially present on the surface of Al powders.[2]

MM processed Al/CNT powders have been consolidated by conventional methods, *e.g.*, hot pressing,[11,12] hot extrusion,[13,14] and spark plasma sintering.[15,16] Since in these techniques densification occurs by heating at relatively high temperatures, an interfacial reaction between Al and CNTs may result in the formation of brittle Al_4C_3 phase.[17] Grain growth of nanocrystalline Al may occur as well. Both have a detrimental effect on the mechanical properties of Al/CNT composites.

Severe plastic deformation (SPD), a top-down approach that applies intense strains to workpiece materials, can be used for production of bulk fully-dense ultrafine-grained materials. Recently, SPD processes like equal channel angular pressing (ECAP),[18,19] accumulative roll bonding (ARB),[20,21] friction stir processing (FSP),[22,23] and high-pressure torsion (HPT)[24,25] have been successfully applied for uniform dispersion of CNTs in Al matrix at room temperature. HPT is especially attractive because it generally produces grains of less than 100 nm, which are significantly smaller than those obtained from the other techniques.[26] In HPT, a disk sample is located between two anvils rotating under a high pressure of several GPa.[27]

The aim of this work is to fabricate fully-dense Al/CNT composites with uniform distribution of CNTs using HPT processing of MM processed Al and CNT powder mixtures. Through an analysis of the microstructure and mechanical properties of the Al/CNT composites, we suggest a strengthening mechanism for CNTs in the Al matrix.

II. EXPERIMENTAL METHOD

Commercial purity Al (99.5 pct, Alpha Industries, South Korea) and MM Al-3 vol pct multi-walled CNT

HAMED ASGHARZADEH, Assistant Professor, is with the Department of Materials Engineering, Faculty of Mechanical Engineering, University of Tabriz, 51666-16471 Tabriz, Iran. Contact e-mail: asgharzadeh@tabrizu.ac.ir SOO-HYUN JOO, Ph.D. Candidate, and HYOUNG SEOP KIM, Professor, are with the Department of Materials Science and Engineering, Pohang University of Science and Technology (POSTECH), Pohang 790-784, South Korea. Contact e-mail: hskim@postech.ac.kr

Manuscript submitted December 20, 2013.
Article published online May 23, 2014

composite (Applied Carbon Nanotechnology Co., South Korea) powders were used as starting materials. Inspection of the powders by field emission scanning electron microscope (FESEM: JEOL JSM-6330F, Japan) (Figure 1) demonstrated an irregular shape for the Al powders and a relatively equiaxed morphology for the Al/CNT powders. The Al/CNT powders consisted of CNTs between welded Al flakes, which is a typical morphology for MM processed composite powders. Approximately 0.3 g of the powders was precompacted under pressure of ~1 GPa into disk-shaped samples with a diameter of 10 mm and thickness of ~1.5 mm. Then, the green compacts were placed between anvils of the HPT facility with a circular shallow hole, 10 mm in diameter and 0.25 mm deep, as illustrated in Figure 2(a). The disks were compressed and deformed under the applied pressure of 6 GPa at room temperature. The rotation of the lower anvil was started after 30 seconds of load application with a rotational speed of 1 rpm and was terminated after various numbers of revolutions up to $N = 15$. The temperature rise during HPT was monitored using a thermocouple placed at 10 mm above the sample. The HPT disks were 10 mm in diameter and ~0.8 mm thick (Figure 2(b)). The same HPT processing was performed on Al powders without CNTs for comparison.

After trimming the flashes, the density of the HPT samples was measured using the Archimedes technique with a Mettler Toledo XP205 density meter by immersing the samples in diethyl phthalate (DEP). The surfaces of the samples were polished to a mirror-like surface with a diamond suspension. The samples were etched using a solution of 1 pct HF in distilled water. The polished and etched surfaces were observed by optical microscope (OM, Olympus BX61, Japan) and SEM (Hitachi SU6600, Japan). For transmission electron microscopy (TEM) examination, the specimens were prepared by dual-beam focused ion beam (FIB) milling using a 3D Total Analysis (Helios Nanolab DualBeam, FEI, Hillsboro, Oregon, USA) cut from the HPT disks at a distance of 2.5 mm from the center. A JEOL JEM 2100F TEM operated at 200 kV, equipped with a high-angle-angular-dark-field (HAADF) detector, was used for scanning transmission electron microscopy (STEM) imaging, acquiring selected-area electron diffraction (SAED) patterns, and high-resolution TEM (HRTEM). Raman spectroscopy was performed by a Senterra spectrophotometer (Bruker, Germany) using a laser wavelength of 532 nm at 10 mW power at room temperature.

Vickers microhardness was measured along the diameter of the polished HPT disks with an applied load of 300 gf (2.94 N) for 10 seconds using a Future-Tech FM-700 tester. Four miniature tensile specimens with a 1.5-mm gage length and 1-mm width (Figure 2(b)) were cut from the HPT disks at a position 2 mm from the center using electro-discharge machining (EDM). For removing surface defects that may be introduced by EDM, the specimens were ground and carefully polished. The tensile tests were performed at room temperature with an initial strain rate of 10^{-3} s^{-1} using an Instron machine (8862 High-Precision Electric Actuator Systems, MA, USA). During the tensile test, precise strains were measured by ARAMIS 5 M (GOM mbH, Germany) vision strain system. Before testing, a random black and white speckled pattern was created on the polished surface of the specimens. Using the digital image correlation (DIC) method, local and global strains were precisely determined. The fracture surfaces of the broken specimens were observed using SEM.

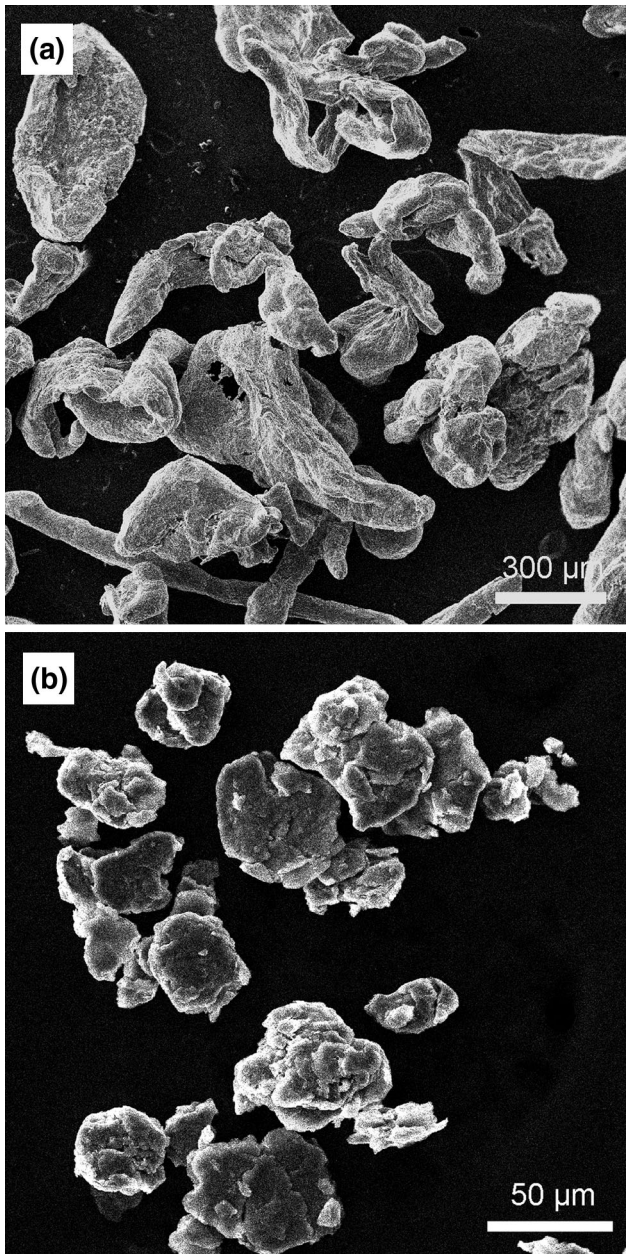

Fig. 1—SEM images of (*a*) Al and (*b*) Al/CNT powders.

III. RESULTS

The densities of Al and Al/CNT subjected to HPT as a function of the number of revolutions are shown in Figure 3. The theoretical density of Al-3 vol pct CNT

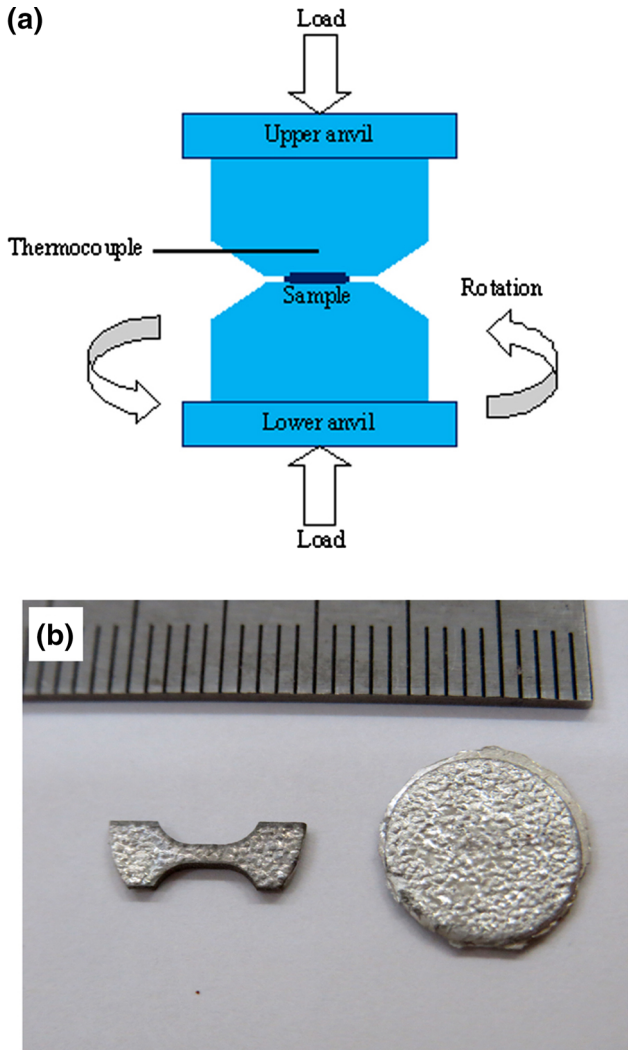

Fig. 2—(*a*) A schematic illustration of the HPT process and (*b*) A HPT disk with a tensile test sample.

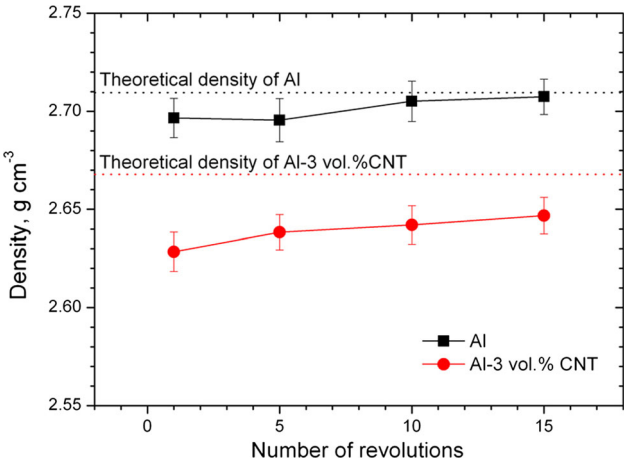

Fig. 3—Variation of density of the HPT-consolidated disks as a function of the number of revolutions.

composite was calculated from the densities of Al (2.71 g cm^{-3}) and CNT (1.33 g cm^{-3}) using the rule of mixtures. The relative green density of Al and Al/CNT compacts was measured 0.984 and 0.971 g cm^{-3}, respectively. A high degree of densification to relative densities of 99.5 and 98.5 pct was achieved after only one revolution for Al and Al/CNT, respectively. The density slightly increased with increasing the number of revolutions.

Figures 4 and 5 illustrate the microstructural evolutions of Al and A/CNT with increasing the number of revolutions, respectively. In Al, there were some large pores and less-deformed particles at the center of the disk after one revolution (Figure 4(a)). However, a few small pores with a low fraction of less-deformed particles appeared in the middle and the edge of the HPT sample (Figures 4(b) and (c)). After 10 revolutions, almost full densification was achieved. There was a whirlpool-like deformation pattern near the center and middle regions of the sample (Figures 4(d) and (e)). Furthermore, prior particle boundaries (PPBs) were not visible and there was essentially a uniform deformation near the edge of the disk (Figure 4(f)). This whirlpool-like deformation was also reported as "double-swirling" by Cao *et al.*[28]

In Al/CNT, while a high fraction of small pores after one revolution, especially in the vicinity of the disk center was observed, there is an insignificant change in the microstructure at different regions of the disk (Figures 5(a) through (c)). Although original particles remained almost undefeated in the center of the disk, they were somehow deformed near the edge of the sample. HPT processing for 10 revolutions imposed a significant deformation on the powder particles so that the PPBs could not be distinguished at both the middle and near the periphery of the disks (Figures 5(e) and (f)).

The detailed microstructure analysis for the HPT-processed Al/CNT sample was conducted using STEM, as presented in Figure 6. The bright-field (BF) and dark-field (HAADF) STEM images (Figures 6(a) and (b)) show a lamellar structure in which the Al grains are elongated along the torsion direction. The distribution of grain sizes measured from 100 grains in the HAADF micrographs revealed that the matrix microstructure was refined to a homogeneous nanograin structure after 10 revolutions by HPT. In perpendicular to the compression axis of HPT, the average grain thickness was about 38 nm, which indicates an aspect ratio of 2.97. The microstructure of pure Al processed by HPT which was explored elsewhere[24] revealed an elongated microstructure with an average grain thickness and length of ~250 and ~530 nm, respectively. Inspection of the BF images discloses that there are many dislocations within the grains. The SAED pattern (shown in Figure 6(a) as an inset) exhibited discrete rings indicating that the nanograins were separated by high angles of misorientations. It should be noted that diffracted beams associated with CNTs are too weak to be detected in the SAED pattern. It can be established from this result that the HPT process introduced a high shear strain in the Al matrix so that a significant grain refinement occurred. Figure 6(d) displays a HRTEM micrograph showing some CNTs with a wall interval of 0.322 nm embedded in the Al matrix. No intermediate compound

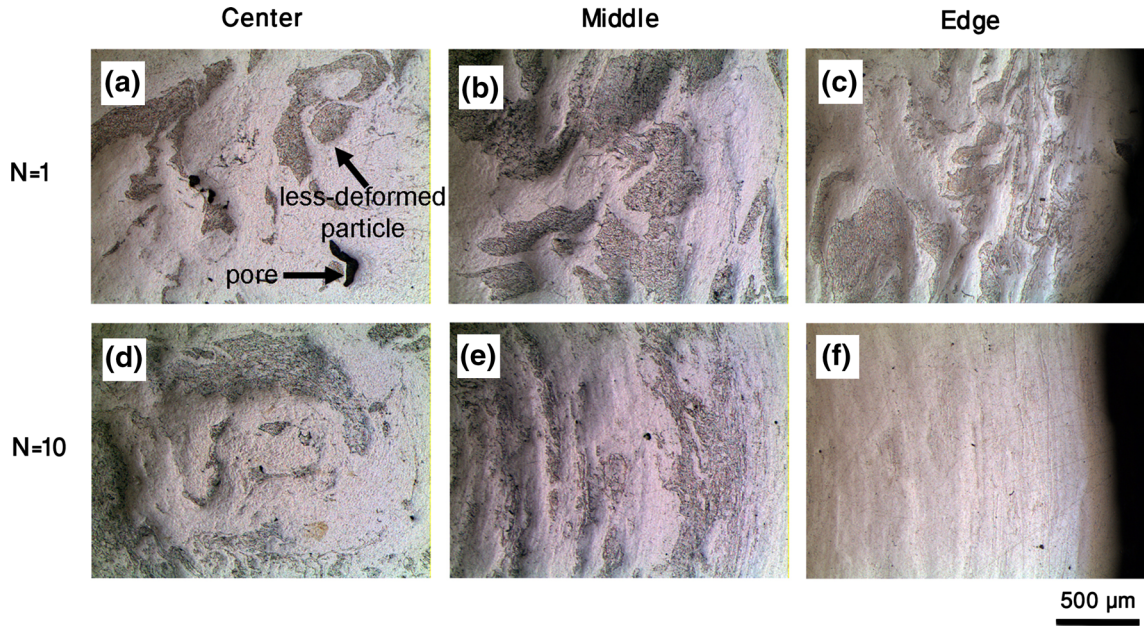

Fig. 4—Optical micrographs from the microstructure of the HPT-processed Al disks: (*a* through *c*) $N = 1$ and (*d* through *f*) $N = 10$ at the center, middle, and edge of the disks.

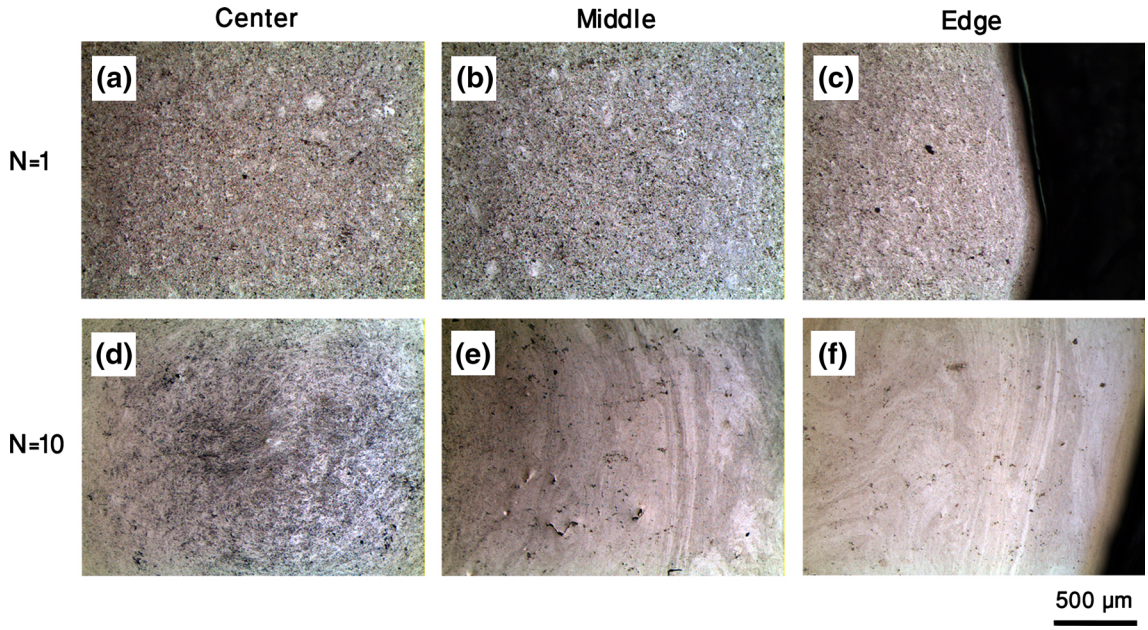

Fig. 5—Optical micrographs from the microstructure of the HPT-processed Al/CNT disks: (*a* through *c*) $N = 1$ and (*d* through *f*) $N = 10$ at the center, middle, and edge of the disks.

was detected by HRTEM at the interfaces, which indicates a good interfacial bonding between CNTs and Al. It is pertinent to point out that some CNTs were broken into fragments during high-energy MM and subsequent HPT processing as revealed by the HRTEM image.

Complementary information about nanotube structure evolution upon the HPT process was attained by Raman spectroscopy. As shown in Figure 7, there were two peaks at ~1337 cm^{-1} (D band) and at ~1566 cm^{-1} (G band) in the Raman spectrum of the CNTs. The D band occurred due to the breathing modes of sp^2 atoms in rings, while the G band resulted from the bond stretching of all pairs of sp^2 atoms in both rings and chains.[29] While there is a slight shift in the wave number of D peak after MM of CNT and Al powder mixture, the wave number of G peak increased to ~1605 cm^{-1}. In addition, there is no shift in the wave number of the D and G peaks at the center and the edge of HPT disks compared to the MM powder. The relative

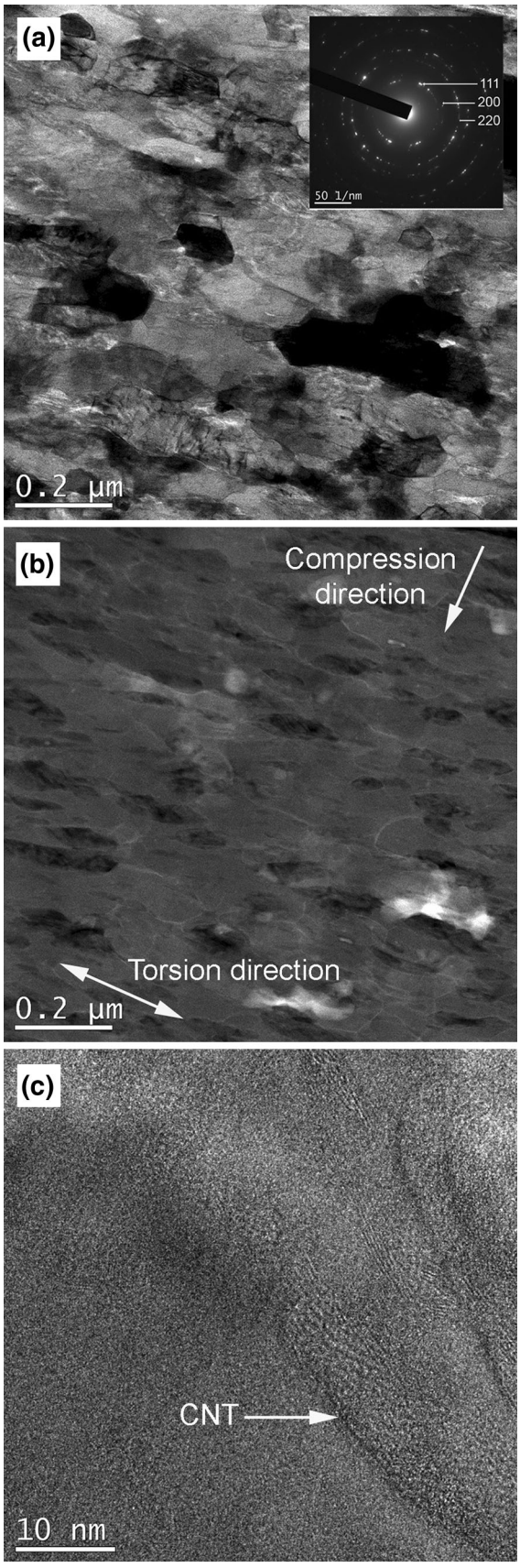

Fig. 6—Microstructure of the Al/CNT composite subjected to HPT for $N = 10$ under $P = 6$ GPa: (*a*) BF image including SAED pattern; (*b*) HAADF image; and (*c*) HRTEM image.

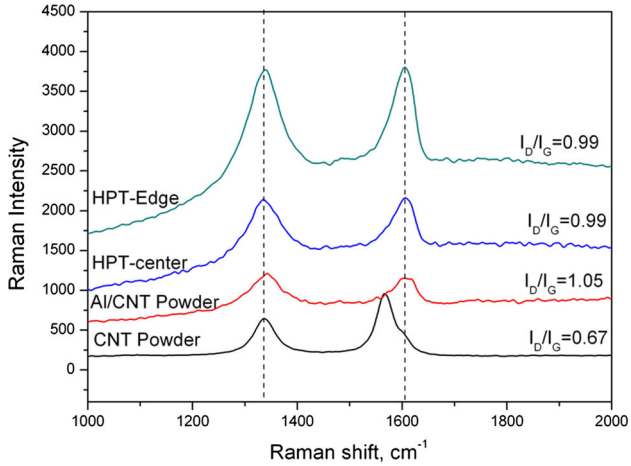

Fig. 7—Raman spectra of CNT powder and the Al/CNT before and after HPT processing for 10 revolutions.

intensity ratio of D to G peak (I_D/I_G), which represents the defect density in graphitic structures, was ~0.67 for the CNT powder. I_D/I_G increased to ~1.05 for Al/CNT powder before HPT and to ~0.99 for that after the HPT process both at central and edge regions. A small change in I_D/I_G without alteration in the peak position after HPT revealed that the CNT graphite structure was slightly damaged during HPT processing.

Figure 8(a) shows variations of Vickers microhardness across the HPT-processed disks with and without CNTs. The hardness level of the Al/CNT composites is significantly superior to that of Al, *e.g.*, the maximum value of the hardness of the Al/CNT sample was 28 pct higher than that of the Al sample. Inspection of microhardness profiles in Figure 8(a) reveals that hardness increased with the distance from the disk center, as is especially evident after one revolution. The regions of higher microhardness near the periphery moved inwards toward the center of the disk so that after 10 revolutions, the local values of microhardness were fairly homogeneous across the sample. The hardness of the Al disks increased gradually with increasing the number of revolutions. On the other hand, the hardness of the Al/CNT disks increased from $N = 1$ to $N = 5$, but it decreased for a larger number of revolutions except at the center of the disks (Figure 8(a)).

The equivalent von Mises strain (ε) can be calculated by Reference 27:

$$\varepsilon = \frac{2\pi N r}{\sqrt{3}t}, \qquad [1]$$

where N is the number of revolutions, r is the distance from the torsion axis (center of the disk), and t is the thickness of the disk. All microhardness values in Figure 8(a) are plotted against von Mises strain in Figure 8(b). It is clear that the hardness increased with increasing equivalent strain at an early stage of straining, but the rate of hardness increase was larger in Al/CNT than in Al. A sudden change in the rate of hardness increase of the Al disks occurs at $\varepsilon \approx 500$.

Nevertheless, there was a maximum hardness of ~122 Hv at $\varepsilon \approx 180$ in the Al/CNT sample. A gradual reduction of the hardness level is noticeable at higher equivalent strains in the Al/CNT composite.

The stress–strain curves for the HPT-processed samples with and without CNTs are presented in Figure 9(a). The Al sample exhibited plastic yielding at 210 MPa followed by strain hardening. Higher yield strength with a limited strain hardening was obtained for the Al/CNT specimen. Figures 9(b) and (c) show DIC results of the tensile test in terms of von Mises strain in the facets on the surfaces of specimens calculated using the data recorded by the ARAMIS measurement system. The Al sample had a high amount of strain which was concentrated on an inclined plane at ~45 deg. Nevertheless, a low strain with a relatively uniform distribution was attained for the Al/CNT composite. Therefore, the Al exhibited high ductility but the Al/CNT composite had low ductility, according to Table I.

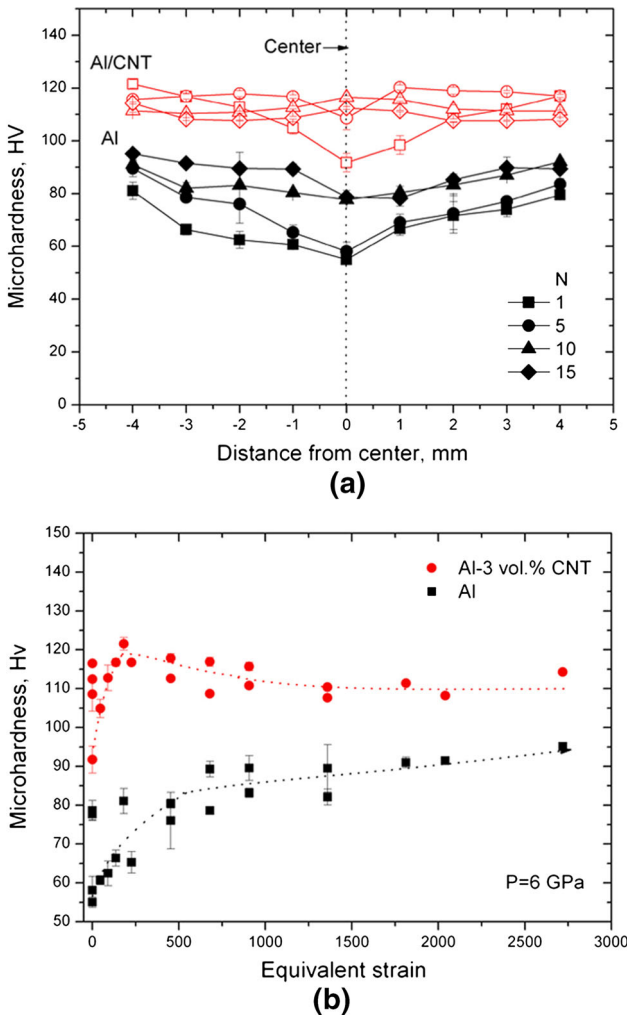

Fig. 8—Vickers microhardness against (*a*) the distance from the center of the disks and (*b*) equivalent strain of Al and Al/CNT samples processed for various numbers of revolutions.

Figure 10 shows SEM images of the tensile fracture surfaces of samples. A ductile fracture with rather fine dimples was observed for Al, as shown in Figure 10(a). On the other hand, the fracture surface of the Al/CNT sample mostly exhibited a smooth fracture manner with many fine dimples (Figure 10(b)). The fracture surface of the composite exhibited no pull-out of CNTs either. It is pertinent to point out that pull-out of CNTs in AMCs results in an inadequate load transfer from the matrix to CNTs, whereas it increases the ductility and fracture toughness of the composite.[30,31]

IV. DISCUSSION

Both commercial purity Al and Al-3 vol pct CNT samples show high densities in the range 98.5 to 99.99 pct of theoretical density due to the large applied pressure and intense strain introduced by HPT processing at room temperature. It is recognized that the temperature is gradually raised during HPT straining that can alter the densification behavior. Experiments and finite element simulations have shown that the temperature increase in processing of pure Al disks by HPT at various applied pressures, rotation rates and the number of turns was less than 328.5 K (55.5 °C).[32] Although the increase of temperature is proportional to the hardness/strength of a material,[32,33] the maximum temperature rise during the processing of Al/CNT samples was measured 313 K (40 °C). Therefore, the effect of temperature increment during straining is expected to have little contribution to the powder consolidation.

In the early stages of HPT processing, the hardness in the center is low due to the small imposed shear strain predicted by Eq. [1]. This also affected the consolidation of the powders so that some porosity remained in the center of the disks. The microstructure was significantly refined, but was heterogeneous at low strain levels (Figures 5 and 6). Therefore, hardness increased with increasing the distance from the center in the early stages of staining (Figure 8(a)). Despite the linear dependence of the strain on the distance from the center according to Eq. [1], the hardness varies in a non-linear manner due to decreasing work hardening with strain.[34] There was a gradual rise in the hardness level and in the microstructural homogeneity with increasing

Table I. Tensile Properties of the HPT-processed Al With and Without CNTs

Material	Yield Strength (MPa)	Ultimate Tensile Strength (MPa)	Elongation (Pct)
Al	210	296	23.1
Al-3 vol pct CNT	280	321	1.4

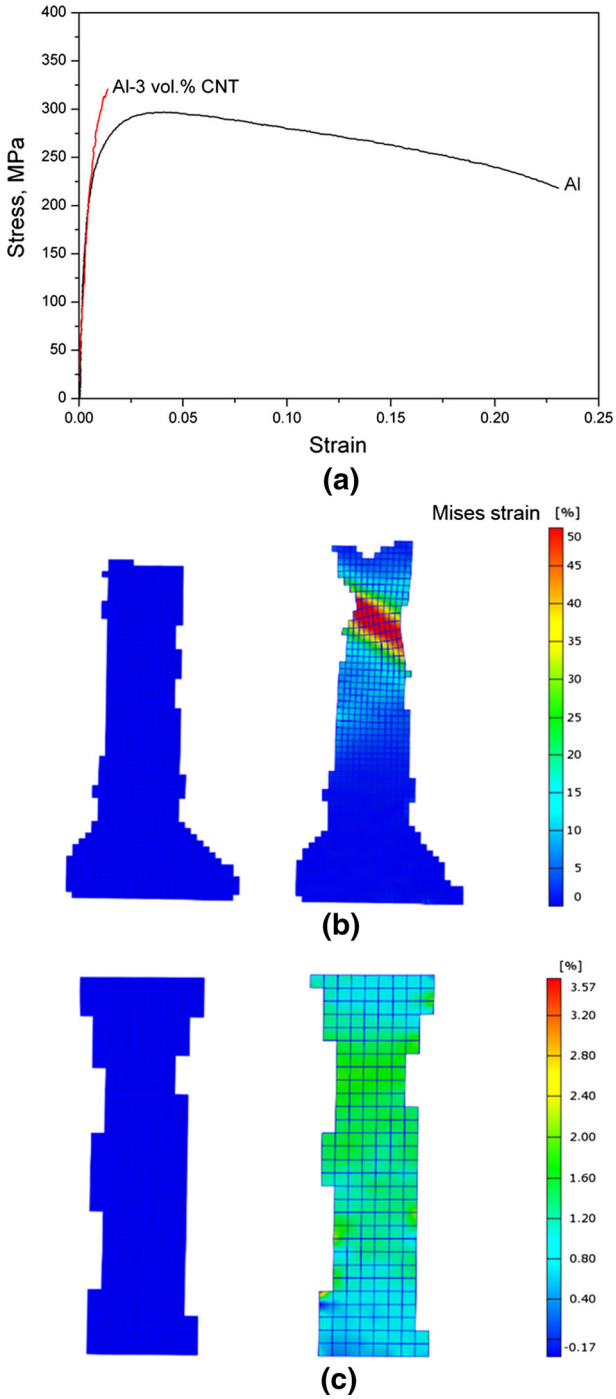

Fig. 9—(*a*) Tensile stress–strain curves and (*b*, *c*) Mises strain distribution for a tensile test before test (left) and before fracture (right); (b) Al; and (c) Al-3 vol pct CNT.

number of revolutions in the commercial purity Al. However, a constant level of microhardness was not fully developed by the extent of strain imposed (Figure 8(b)), in contrast to the previous studies of HPT processing on commercial purity Al.[24,35,36] This behavior has been observed in materials with low stacking fault energies and/or slow recovery rates like Al alloys (*e.g.*, Al6061[37] and Al-1 pct Mg[36]) in which microstructural evolution occurs at a slow rate during

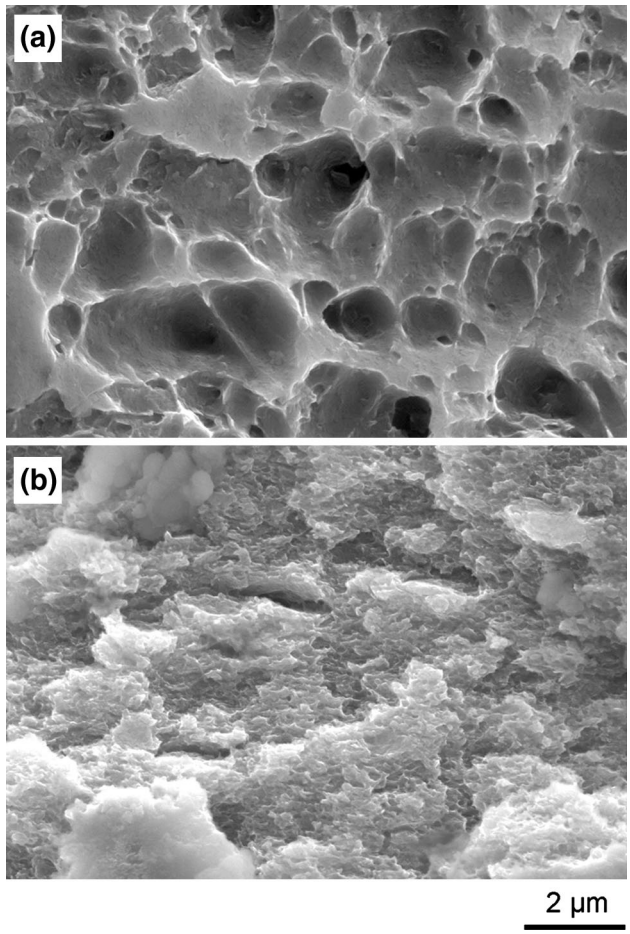

Fig. 10—Fracture surfaces of tensile specimens: (*a*) Al and (*b*) Al/CNT.

HPT and higher imposed strains are needed in order to achieve microstructural homogeneity.[38] In this case, the presence of alumina layer on the Al powders which were dispersed in the Al matrix through the HPT process can reduce recovery rates by hindering the dislocation motions. After processing to high strain levels, the subgrain boundary misorientation increased, but heterogeneous microstructure remained. Further torsion up to some tens of revolutions may lead to saturation in the microstructure characteristics and homogenization in the entire cross-section. In contrast to the Al, hardness of the Al/CNT samples was uniformed after 10 revolutions under a pressure of 6 GPa (Figure 8(a)). This is in agreement with the experimental data reported earlier on the dependence of hardness along the radius of MM + HPT-processed Al-5 vol pct CNT[24] and Cu-1 wt. pct CNT[39] samples. On the other hand, the saturation has not been reported in Al-5 wt. pct CNT after processing by HPT for $N = 30$ under $P = 2.5$ GPa.[25] Here, it is pertinent to note that MM prior to HPT has a significant role on microstructural homogeneity and hardness saturation. The grain refinement and reinforcement distribution mechanisms during high-energy MM in AMCs were reported elsewhere.[40] In fact, MM + HPT brings a drastic reduction in grain

size with much more uniform microstructure. A slight decrease in the hardness level at a higher number of revolutions is mainly attributed to an increase in the fraction of damaged CNTs that were bent or broken through HPT (Figure 7).

The hardness and strength values of the Al/CNT were higher than those of Al without CNTs (Figure 8 and Table I). Three strengthening mechanisms can be considered for the Al/CNT composite including (1) Al matrix grain size refinement, (2) dislocation related strengthening such as thermal mismatch between CNTs and the Al matrix or Orowan looping, and (3) load transfer from the Al matrix to the CNTs.

A high degree of grain refinement during HPT results in a significant strengthening. The grain refinement mechanism during the HPT process can be interpreted by a number of physical models. According to the conventional dislocation theory,[41–43] at a low number of revolutions, a very high dislocation density is introduced. CNTs impede the dislocation motion and a high density of dislocation is accumulated. The dislocation accumulation leads to the formation of an intragranular structure consisting of cells with thick cell walls and low angles of grain boundary misorientation. As the strain increases, the thickness of the cell walls decreases and the walls evolve into grain boundaries. Finally, an array of ultrafine grains with high-angle grain boundaries is formed.[44] It should be noted that the average grain size of Al-3 vol pct CNT in this study (~65 nm) was much smaller than those of the HPT-processed Al/CNT composites reported previously.[24,25]

It is well established that the formation of geometrically necessary dislocations (GNDs) as a result of the coefficient of thermal expansion (CTE) mismatch between Al matrix and CNTs increases the strength of the Al/CNT composite.[45,46] In this study, however, Al/CNT composites were processed at relatively low temperatures [<353 K (<80 °C)]. Therefore, strengthening by thermal mismatch strain can be considered minimal due to the low density of GNDs. It is interesting that the hardness level of the Al specimen in this study was significantly (~40 pct) higher than that of the bulk Al sample processed by HPT in previous reports.[35,36] This difference is mainly due to the *in situ* formed Al_2O_3 particles dispersed in the Al matrix through the HPT process. A similar result was reported on the HPT process of high-purity Al by Tokunaga *et al.*[47] The role of *in situ* formed oxide particles on grain refinement and strengthening explained elsewhere.[40,48] The motion of the dislocations is hindered by CNTs and dispersed *in situ* formed Al_2O_3 particles leading to bending of these dislocations between the obstacles and to the formation of dislocation loops.[49] This produces a back stress that will prevent further dislocation migration and results in an increase in the yield strength.[45]

For the Al/CNT composites, an applied force can be transmitted from the Al matrix to the CNTs by means of shear stresses developed along the interface of CNTs and Al. The yield strength of Al/CNT composites is strongly related to the CNTs length (l) and can be estimated by the Kelly-Tyson formula,[50] expressed as

$$\sigma_{Al/CNT} = \sigma_{CNT} f_{CNT} \left(\frac{l}{2l_c} \right) + \sigma_{Al} f_{Al}, \qquad [2]$$

where σ_{CNT} and σ_{Al} are the strengths of CNTs (= 30 GPa) and the Al matrix, respectively, f_{CNT} and f_{Al} are the volume fractions of CNTs and the Al matrix, respectively, l is the average length of CNTs (~10 μm) and l_c is the critical length. l_c is the minimum CNT length necessary to carry the maximum stress at its midpoint and can be given as[13]

$$l_c = \frac{d\sigma_{CNT}}{k\sigma_{Al}}, \qquad [3]$$

where d is the diameter of CNTs (5 to 20 nm) and k is the load-transfer efficiency. The load-transfer efficiency is mostly below one due to the weak interfacial bonding or the peculiar deformation behavior of the matrix.[13] By considering the experimental data, the critical length of CNTs and the load-transfer efficiency were calculated ~59 μm and 3 pct, respectively. Thus, the load transfer from the Al matrix to the CNTs had a slight contribution to the strength of A/CNT. Consequently, it can be considered that the Al/CNT composite was mainly strengthened by Al matrix grain refinement and the Orowan looping of the matrix.

It is reasonable to mention that while nanocrystalline materials generally possess lower tensile ductility compared to coarse-grained counterparts due to the plastic instability, crack nucleation, shear instability, and processing artifacts, *e.g.*, pores,[51] the observed high ductility in our HPT-processed nanocrystalline Al is interesting. Moreover, the large strain is confined to narrow shear bands which are mostly declined to the vertical tensile axis by about 45 deg (Figure 9(b)). Nevertheless, low ductility with flat fracture surface normal to the tensile direction was observed in Al/CNT (Figure 9(c)). It can be due to the fact that dislocations are accumulated or tangled during plastic deformation, leading to large strain localization near CNTs, especially CNT agglomerates which act as stress concentrators. Intense strain localization near nanotubes eventually causes matrix cracking due to severe modulus mismatch between Al and CNT and hence ductile yielding behavior is significantly reduced.[52,53]

V. CONCLUSIONS

HPT was applied to consolidate a MM processed Al and CNT powder mixture. The following conclusions were reached.

1. Almost full densification was achieved in the Al/CNT composite due to the large applied pressure and intense shear strain introduced by HPT at room temperature.
2. CNTs were well dispersed and bonded with the Al matrix. In spite of the distortions of CNTs during processing, load transfer from the Al matrix to the CNTs occurred.

3. A significant Al matrix grain refinement with an average grain size of ~65 nm was obtained, which is attributed to the presence of CNTs and *in situ* formed Al_2O_3 particles.
4. Evaluating the mechanical properties of the Al/CNT composites indicated an improvement of 33 pct in yield stress and 27 pct in hardness over the unreinforced Al.
5. The strengthening of the Al/CNT composite was found to be caused by a synergistic effect of load transfer from the Al matrix to the CNTs, grain refinement strengthening of the Al matrix, and the Orowan looping strengthening due to CNTs and Al_2O_3 particles.

ACKNOWLEDGMENTS

This study was supported by A.D.D. through basic research Project (11-01-04-08). H.A. acknowledges the support of his visiting fellowship by the POSTECH Basic Science Research Institute Grant.

REFERENCES

1. V.N. Popov: *Mater. Sci. Eng. R*, 2004, vol. 43, pp. 61–102.
2. D. Poirier, R. Gauvin, and R.A.L. Drew: *Compos. A*, 2009, vol. 40, pp. 1482–89.
3. J.Z. Liao and M.J. Tan: *Powder Technol.*, 2011, vol. 208, pp. 42–48.
4. C. He, N. Zhao, C. Shi, X. Du, J. Li, H. Li, and Q. Cui: *Adv. Mater.*, 2007, vol. 19, pp. 1128–32.
5. D.H. Nam, S.I. Cha, B.K. Lim, H.M. Park, D.S. Han, and S.H. Hong: *Carbon*, 2012, vol. 50, pp. 2417–23.
6. H. Kwon, M. Estili, K. Takagi, T. Miyazaki, and A. Kawasaki: *Carbon*, 2009, vol. 47, pp. 570–77.
7. C. Suryanarayana: *Prog. Mater Sci.*, 2001, vol. 46, pp. 1–184.
8. H. Asgharzadeh, A. Simchi, and H.S. Kim: *Metall. Mater. Trans. A*, 2011, vol. 42A, pp. 816–24.
9. H. Abdoli, H.R. Farnoush, H. Asgharzadeh, and S.K. Sadrnezhaad: *Powder Metall.*, 2011, vol. 54, pp. 24–29.
10. J.B. Fogagnolo, F. Velasco, M.H. Robert, and J.M. Torralba: *Mater. Sci. Eng. A*, 2003, vol. 342, pp. 131–43.
11. C.L. Xu, B.Q. Wei, R.Z. Ma, J. Liang, X.K. Ma, and D.H. Wu: *Carbon*, 1999, vol. 37, pp. 855–58.
12. R. Zhong, H. Cong, and P. Hou: *Carbon*, 2003, vol. 41, pp. 848–51.
13. L. Jiang, Z. Li, G. Fan, L. Cao, and D. Zhang: *Carbon*, 2012, vol. 50, pp. 1993–98.
14. A.M.K. Esawi, K. Morsi, A. Sayed, M. Taher, and S. Lanka: *Compos. Sci. Technol.*, 2010, vol. 70, pp. 2237–41.
15. D.H. Nam, Y.K. Kim, S.I. Cha, and S.H. Hong: *Carbon*, 2012, vol. 50, pp. 4809–14.
16. A.M. Al-Qutub, A. Khalil, N. Saheb, and A.S. Hakeem: *Wear*, 2013, vol. 297, pp. 752–61.
17. L. Ci, Z. Ryu, N.Y. Jin-Phillipp, and M. Rühle: *Acta Mater.*, 2006, vol. 54, pp. 5367–75.
18. R. Derakhshandeh and A Jenabali Jahromi: *Mater. Des.*, 2011, vol. 32, pp. 3377–88.
19. P. Quang, Y.G. Jeong, S.C. Yoon, S.H. Hong, and H.S. Kim: *J. Mater. Process. Technol.*, 2007, vols. 187–188, pp. 318–20.
20. D. Lahiri, S.R. Bakshi, A.K. Keshri, Y. Liu, and A. Agarwal: *Mater. Sci. Eng. A*, 2009, vol. 523, pp. 263–70.
21. S. Salimi, H. Izadi, and A.P. Gerlich: *J. Mater. Sci.*, 2011, vol. 46, pp. 409–15.
22. H. Izadi and A.P. Gerlich: *Carbon*, 2012, vol. 50, pp. 4744–49.
23. Z.Y. Liu, B.L. Xiao, W.G. Wang, and Z.Y. Ma: *Carbon*, 2012, vol. 50, pp. 1843–52.
24. S.-H. Joo, S.C. Yoon, C.S. Lee, D.H. Nam, S.H. Hong, and H.S. Kim: *J. Mater. Sci.*, 2010, vol. 45, pp. 4652–58.
25. T. Tokunaga, K. Kaneko, and Z. Horita: *Mater. Sci. Eng. A*, 2008, vol. 490, pp. 300–04.
26. D.C. Patil, S.A. Kori, K. Venkateswarlu, G. Das, S.N. Alhajeri, and T.G. Langdon: *J. Mater. Sci.*, 2013, vol. 48, pp. 4773–79.
27. A.P. Zhilyaev and T.G. Langdon: *Prog. Mater Sci.*, 2008, vol. 53, pp. 893–979.
28. Y. Cao, Y.B. Wang, R.B. Figueiredo, L. Chang, X.Z. Liao, M. Kawasaki, W.L. Zheng, S.P. Ringer, T.G. Langdon, and Y.T. Zhu: *Acta Mater.*, 2011, vol. 59, pp. 3903–14.
29. C. Casiraghi, A.C. Ferrari, and J. Robertson: *Phys. Rev. B*, 2005, vol. 72, pp. 085401/1–14.
30. H.J. Choi, J.H. Shin, and D.H. Bae: *Compos. A*, 2012, vol. 43, pp. 1061–72.
31. C.F. Deng, D.Z. Wang, X.X. Zhang, and A.B. Li: *Mater. Sci. Eng. A*, 2007, vol. 444, pp. 138–45.
32. R.B. Figueiredo, P.H.R. Pereira, M.T.P. Aguilar, P.R. Cetlin, and T.G. Langdon: *Acta Mater.*, 2012, vol. 60, pp. 3190–98.
33. K. Edalati, R. Miresmaeili, Z. Horita, H. Kanayama, and R. Pippan: *Mater. Sci. Eng. A*, 2011, vol. 528, pp. 7301–05.
34. P. Jenei, E.Y. Yoon, J. Gubicza, H.S. Kim, J.L. Lábár, and T. Ungár: *Mater. Sci. Eng. A*, 2011, vol. 528, pp. 4690–95.
35. A.P. Zhilyaev, K. Oh-ishi, T.G. Langdon, and T.R. McNelley: *Mater. Sci. Eng. A*, 2005, vols. 410–411, pp. 277–80.
36. M. Kawasaki, S.N. Alhajeri, C. Xu, and T.G. Langdon: *Mater. Sci. Eng. A*, 2011, vol. 529, pp. 345–51.
37. C. Xu, Z. Horita, and T.G. Langdon: *Acta Mater.*, 2008, vol. 56, pp. 5168–76.
38. C. Xu, Z. Horita, and T.G. Langdon: *Acta Mater.*, 2007, vol. 55, pp. 203–12.
39. H. Li, A. Misra, Y. Zhu, Z. Horita, C.C. Koch, and T.G. Holesinger: *Mater. Sci. Eng. A*, 2009, vol. 523, pp. 60–64.
40. H. Asgharzadeh, A. Simchi, and H.S. Kim: *Mater. Sci. Eng. A*, 2010, vol. 527, pp. 4897–905.
41. A.S. Argon and P. Haasen: *Acta Metall. Mater.*, 1993, vol. 41, pp. 3289–306.
42. R.Z. Valiev, Y.V. Ivanisenko, E.F. Rauch, and B. Baudelet: *Acta Mater.*, 1996, vol. 44, pp. 4705–12.
43. M. Zehetbauer and V. Seumer: *Acta Metall. Mater.*, 1993, vol. 41, pp. 577–88.
44. X.G. Qiao, N. Gao, and M.J. Starink: *Philos. Mag.*, 2012, vol. 92, pp. 446–70.
45. R. George, K.T. Kashyap, R. Rahul, and S. Yamdagni: *Scripta Mater.*, 2005, vol. 53, pp. 1159–63.
46. R. Vogt, Z. Zhang, Y. Li, M. Bonds, N.D. Browning, E.J. Lavernia, and J.M. Schoenung: *Scripta Mater.*, 2009, vol. 61, pp. 1052–55.
47. T. Tokunaga, K. Kaneko, K. Sato, and Z. Horita: *Scripta Mater.*, 2008, vol. 58, pp. 735–38.
48. H. Asgharzadeh, A. Simchi, and H.S. Kim: *Mater. Charact.*, 2013, vol. 75, pp. 108–14.
49. E. Orowan: *Z Phys.*, 1934, vol. 89, pp. 634–59.
50. T.H. Courtney: *Mechanical Behavior of Materials*, McGraw-Hill Book Co., Singapore, 2000.
51. M.A. Meyers, A. Mishra, and D.J. Benson: *Prog. Mater Sci.*, 2006, vol. 51, pp. 427–556.
52. H.J. Choi, J.H. Shin, and D.H. Bae: *Compos. Sci. Technol.*, 2011, vol. 71, pp. 1699–705.
53. K. Prashantha, J. Soulestin, M.F. Lacrampe, P. Krawczak, G. Dupin, and M. Claes: *Compos. Sci. Technol.*, 2009, vol. 69, pp. 1756–63.